IEEE Photonics Journal
An IEEE Photonics Society Publication

Open Access

A Photonics-Based Coherent Dual-Band Radar for Super-Resolution Range Profile

Volume 11, Number 4, August 2019

Shaowen Peng
Shangyuan Li
Xiaoxiao Xue
Xuedi Xiao
Dexin Wu
Xiaoping Zheng

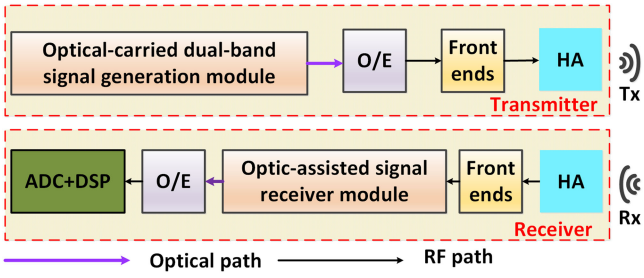

DOI: 10.1109/JPHOT.2019.2929210

IEEE photonics SOCIETY
IEEE

A Photonics-Based Coherent Dual-Band Radar for Super-Resolution Range Profile

Shaowen Peng, Shangyuan Li, Xiaoxiao Xue, Xuedi Xiao, Dexin Wu, and Xiaoping Zheng

The authors are with the Beijing National Research Center for Information Science and Technology, Department of Electronic Engineering, Tsinghua University, Beijing 100084, China

DOI:10.1109/JPHOT.2019.2929210
This work is licensed under a Creative Commons Attribution 4.0 License. For more information, see https://creativecommons.org/licenses/by/4.0/

Manuscript received June 29, 2019; accepted July 13, 2019. Date of publication July 17, 2019; date of current version July 29, 2019. This work was supported in part by the National Nature Science Foundation of China (NSFC) under Grants 61690191, 61690192, 61420106003, and 61621064 and in part by Chuanxin Funding; Beijing Natural Science Foundation under Grant 4172029. Corresponding author: Xiaoping Zheng (e-mail: xpzheng@mail.tsinghua.edu.cn).

Abstract: We propose and demonstrate a photonics-based coherent dual-band radar for super-resolution range profile in this paper. This radar cannot only generate coherent dual-band linear frequency modulated signals with large bandwidths, but also realize a paralleled coherent de-chirping processing to the dual-band echoes simultaneously based on a single compact photonics-assisted transceiver. The sharing of a single transceiver for signals with different bands ensures perfect stability and coherence among the waveforms, which makes it possible to realize a super-resolution range profile by fusion of dual-band signals without heavy computation on phase compensation. In the experiment, the radar operates in *S*-band with a bandwidth of 1.5 GHz and *X*-band with a bandwidth of 3 GHz, and results show its range resolution is up to 1.6 cm by coherent fusion processing, which is nearly corresponding to the resolution gotten by a linear frequency modulated wave with a bandwidth of 9.5 GHz ranging from 2 GHz to 11.5 GHz, much higher than the scenario when the radar is operated in the single-band mode. This technology would improve the accuracy of classification and recognition of the targets.

Index Terms: Photonics, dual-band radar, super-resolution range profile.

1. Introduction

Radar system is an efficient method to detect the targets in all-weather conditions [1]. With the external space environment getting more and more complex, higher requirements on radar detection capabilities are demanded, such as the high range resolution. High-resolution range profile (HRRP) is one of the most important signatures of the targets and it has been applied in the field of automatic target recognition. As we can know, the higher the range resolution is, the higher the recognition accuracy is. The straight method to improve the range resolution of the radar is to extend the instantaneous bandwidth of the transmitted signal [2]. However, due to the electronic device bottlenecks, the bandwidth of the traditional electronic radar is limited [3], [4]. During the past few years, microwave photonic technology offers a promising solution to the problem for its unique features of wide bandwidth, high frequency, immunity to electromagnetic interference and so on [5]–[7]. Many photonics-based methods have been proposed for generating and processing microwave signals with a large time-bandwidth product (TBWP). In terms of signal generation, the main methods include frequency multiplication [8], [9], photonic digital-to-analog converter

(PDAC) [10], [11] and photonic up-conversion [12]–[17]. Regarding the processing of the received signals, photonic de-chirping processing [8], [11] and photonic analog-to-digital converter [18] have been proposed with good performance. Based on these technologies, several typical photonics-based radar systems working at a wide band have been demonstrated and the range resolution of several centimeters are realized in the experiments [8], [11]. However, due to the strict control of electromagnetic spectrum resource utilization, these radar systems are not permitted to work in an ultra-wide band. Otherwise, it is easily interfered by other devices when their working frequency bands overlap. Besides, it is still difficult for the radio frequency (RF) front-ends to process these signals with an ultra-wide bandwidth.

Another method to improve the range resolution of the radar is coherent fusion processing of the multiband radar signals. Until now, lots of simulations have verified their feasibilities [19]–[25]. The missing band signal between the dual-band signals can be interpolated and an improved resolution range profile can be obtained based on ultra-wideband coherent fusion processing. However, there are several defects limiting the implementation of the actual traditional dual-band radar system for super-resolution range profile. Due to the electronic device bottlenecks, the traditional dual-band radar system consists of two distinct radar systems working in different bands, leading to a significant increase of the cost and complexity [14]. Besides, the resolution of the range profile realized by these systems is in the order of decimeter limited by the working bandwidth. For example, in [23], the range resolution is only about 25 cm. What's more, due to the phase drifts of the local oscillators and the use of noisy electronic mixers in the distinct sub-band radar systems, the generated signals at different bands are incoherent [16], which makes the fusion processing complex or even invalid.

In this paper, in order to solve the problems mentioned above, a photonics-based dual-band radar for super-resolution range profile is proposed and demonstrated. Based on a single transceiver, this system can not only generate coherent dual-band signals with large bandwidths, but also realize the parallel coherent de-chirping processing to the dual-band echoes simultaneously, which makes the super-resolution range profile of targets by coherent fusion processing of the dual-band signals possible. In the experiment, a dual-band radar operating in the S-band with a bandwidth of 1.5 GHz (2–3.5 GHz) and X-band with a bandwidth of 3 GHz (8.5–11.5 GHz) is established. By performing coherent fusion processing, a super-resolution can be obtained, which is corresponding to the resolution gotten by a linear frequency modulated wave (LFMW) with a bandwidth of 9.5 GHz ranging from 2 GHz to 11.5 GHz. The radar system is evaluated through range profiles of two metallic plane targets and the super range resolution of 1.6 cm is demonstrated. To the best of our knowledge, it is higher than the resolution realized by other reported dual-band radar systems [16], [23].

2. Topology and Operation Principle

Figure 1(a) shows the schematic diagram of the proposed photonics-based dual-band radar system. In the transmitter, a combination of two optical-carried LFMWs at different band is generated from the optical-carried dual-band signal generation module. Then the optical signal is converted into an RF dual-band LFMW signal through the optical to electrical converter (O/E). The output photo-current of the O/E module can be expressed as

$$I(t) = \sum_{i=1}^{2} rect\left(\frac{t}{T_{p_i}}\right) A_i \exp\left(j2\pi\left(f_i t + \frac{1}{2}k_i t^2\right)\right), \tag{1}$$

where $i(i = 1, 2)$ stands for the two LFMWs separately, T_{p_i} is the pulse width, f_i is the carrier frequency, k_i is the chirp rate and A_i is the amplitude. The dual-band signals are characterized by a strict phase coherent. After filtered and amplified by the fronts end, the dual-band signal is emitted to the free space through a horn antenna (HA). In the receiver, the echoes at different bands reflected from the targets are received by HAs. Then they are filtered and amplified by the front ends. After that, the signals are injected into an optic-assisted signal receiver module (OSRM). This OSRM is mainly to realize parallel de-chirping processing. After optical to electrical conversion in

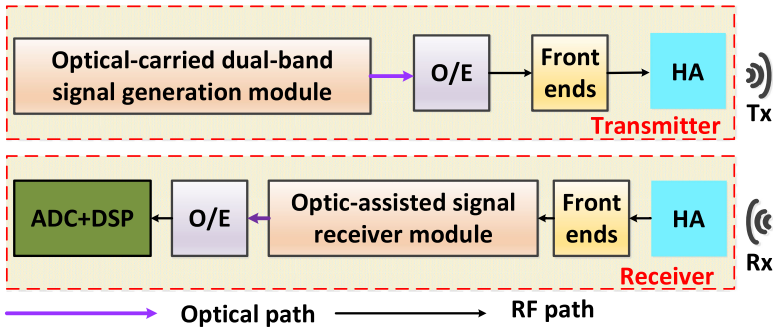

Fig. 1. Schematic diagram of the proposed dual-band radar system. O/E: optical to electrical converter; HA: horn antenna; ADC: analog to digital converter; DSP: digital signal processor.

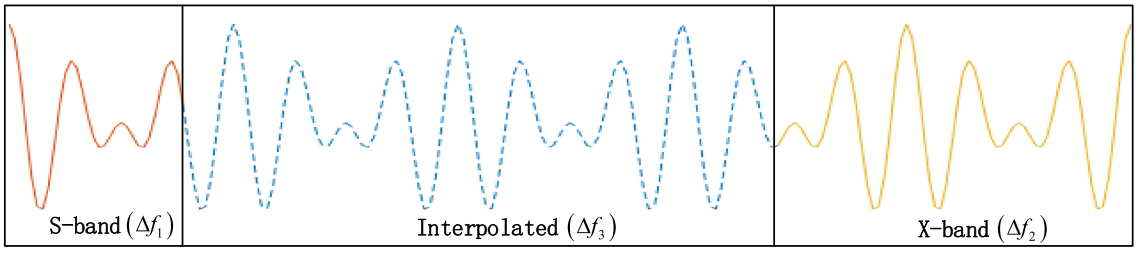

Fig. 2. Coherent fusion processing concept applied to band-1 and band-2 wideband data.

an O/E, the de-chirped signals can be obtained. The output photo-current of the O/E module can be expressed as

$$I_{dechirp\_i}(t) \propto \cos\left(2\pi k_i \tau t - \pi k_i \tau^2 + 2\pi f_i \tau\right), \tag{2}$$

where $i (i = 1, 2)$ stands for the two band signals separately, and τ is the time delay of the echo wave. The two de-chirped signals still maintain a phase coherence, which reduces the complexity of the phase compensation. Each of the de-chirped signals is then digitized by a low-speed analog-to-digital converter (ADC). Finally, a DSP unit is used to process the digital signal, including data fusion processing. According to [2], the range resolution is $\delta_r = c/2B$, where c is the velocity of light and B is the bandwidth of the signal. Due to the large bandwidth of the dual-band signal, each single-band radar can realize an HRRP, guaranteeing the realization of super-resolution range profile by coherent fusion processing. Besides, parallel de-chirped processing transforms the broad-band signal to a narrow-band signal, allowing digitization with a low-speed ADC and thus reducing the complexity of the system.

A high-resolution range profile of targets can be obtained by coherent fusion processing of the dual-band signals. It is known that the scattering character of the individual scattering centers varies significantly in a wideband frequency. If a model can be constructed from sub-bands data to describe the scattering character, the missing data between the sub-bands can be obtained [20]. As shown in Fig. 2, there are two band signals, named band-1 and band-2, whose bandwidths are Δf_1 and Δf_2. Accordingly, the resolution of the two band signals are $\delta_{r1} = c/2\Delta f_1$ and $\delta_{r2} = c/2\Delta f_2$ separately. Since these two band signals can be measured, the missing band signal with a bandwidth of Δf_3 between the band-1 and band-2 signal can be obtained through interpolation. Then a whole band signal from band-1 to band-2 can be obtained. When the model of the algorithm can match the target scattering characteristics very well, the effective bandwidth of the fusion data can be up to $\Delta f = \Delta f_1 + \Delta f_2 + \Delta f_3$, and the super range resolution can be expressed as

$$\delta_r = \frac{c}{2\left(\Delta f_1 + \Delta f_2 + \Delta f_3\right)} \tag{3}$$

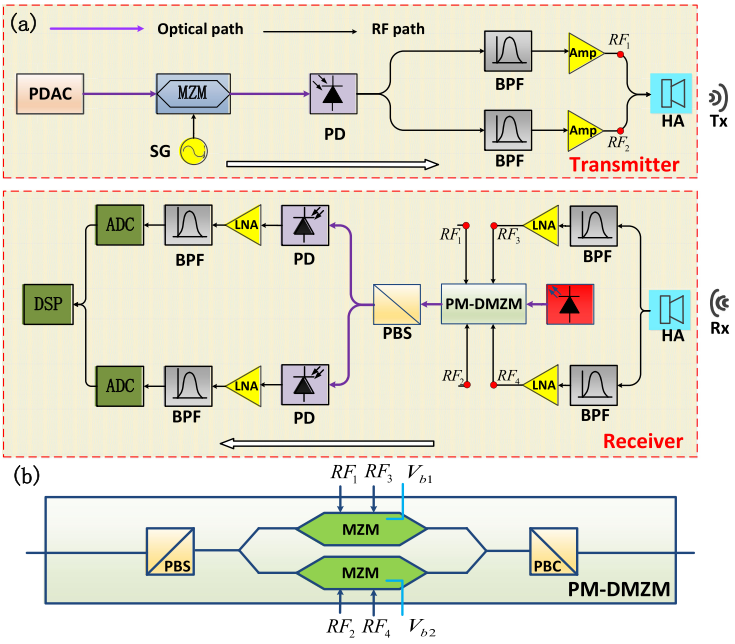

Fig. 3. (a) The experiment setup of the proposed dual-band radar system. (b) The detailed structure of the PM-DMZM. PDAC: photonic digital-to-analog converter; MZM: Mach-Zehnder modulator; SG: signal generator; PD: photodetector; BPF: band-pass filter; Amp: amplifier; HA: horn antenna; PM-DMZM: polarization-multiplexing dual driving Mach-Zehnder modulator; PBC: polarization beam combiner; PBS: polarization beam splitter; LNA: low-noise amplifier; ADC: analog to digital converter; DSP: digital signal processor.

It should be noted that when the missing band is too large compared to the sum of the sub-bandwidth, the model of the algorithm cannot match the target scattering characteristics well, thus the range resolution of δ_r will not be available.

3. Experiment and Discussion

To evaluate the performance of the proposed dual-band coherent radar, an experiment is conducted and the experiment setup is shown in Fig. 3. In the transmitter, the optical-carried dual-band signal generation module is realized by a PDAC and a Mach-Zehnder modulator (MZM). A combination of two optical-carried LFMWs is generated from a 4-bit PDAC, which has been proposed in our previous work [11]. Due to the broadband characteristics of the PDAC, two optical-carried LFMWs with large bandwidths can be generated from it. Since the two LFMWs are all generated by the PDAC at the same time, there is a fixed phase relationship between them. Both the LFMWs have a time duration of 8 μs and a period of 10 μs and are centered at $f_1 = 2.75$ GHz and $f_2 = 6$ GHz with a bandwidth of 1.5 GHz and 3 GHz separately. Then the optical signal is injected into an MZM (AVANEX SD40), which is biased at orthogonal transmission point and driven by a local oscillator with a frequency of 16 GHz from an SG (Agilent E8403A). Thus, an optical-carried LFMWs replica is generated. It is easy to adjust the repeat frequency of the optical signal by adjusting the frequency of the driving signal for the wide working bandwidth of the MZM. Then the output light from the MZM is injected into a photodetector (PD). After the square-law detection, a multi-band LFMW is obtained. Subsequently, the signal is selected by two band-pass filters (BPFs), whose pass band range are 2–4 GHz and 8–12 GHz separately. After that, the generated S-band and X-band signals with a strict phase coherence are both amplified and split into two parts by couplers separately. One is sent to a polarization-multiplexing dual driving Mach-Zehnder modulator (PM-DMZM) as a reference signal, the other is coupled and emitted to the free space through an HA.

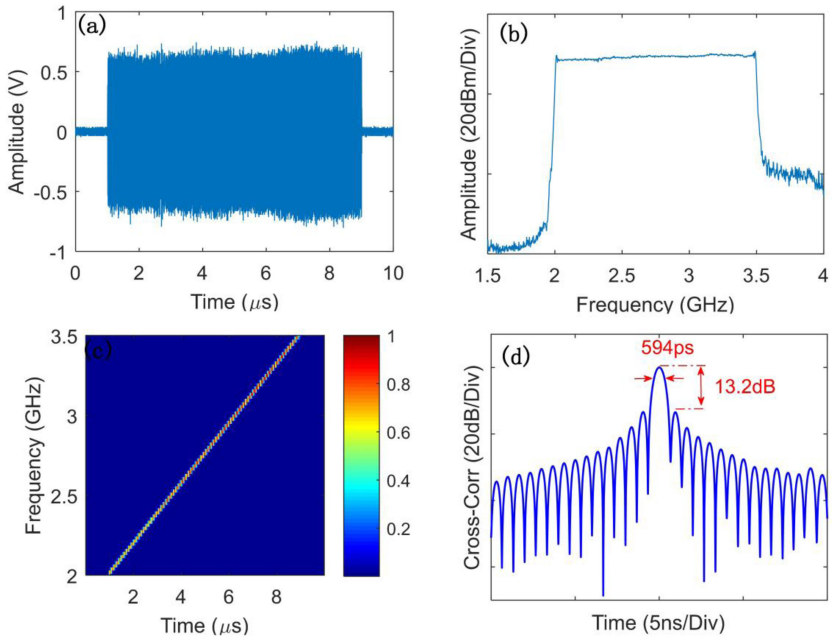

Fig. 4. Generation of the S-band LFMW with a bandwidth of 1.5 GHz (2–3.5 GHz), a pulse width of 8 μs and a period of 10 μs. (a) The waveform, (b) the spectrum, (c) the instantaneous frequency and (d) the cross-correlation peak.

The S-band and X-band LFMWs are measured at the output point of each amplifier separately in the transmitter shown in Fig. 3 by an oscilloscope (Agilent DSO81204B) and a spectrum analyzer (Agilent E4446). Figures 4 and 5 show the results of the S-band signal with a bandwidth of 1.5 GHz (2–3.5 GHz) and X-band signal with a bandwidth of 3 GHz (8.5–11.5 GHz), separately. Both the signals have a pulse width of 8 μs and a period of 10 μs. Figures 4 and 5(a), (b), (c) and (d) are waveform, spectrum, instantaneous frequency and cross-correlation peak with corresponding ideal signal separately. As for ideal LFMW with the same parameter as the generated S-band signal, the full-width at half maximum (FWHM) of the compressed pulse is about 590 ps and the peak sidelobe ratio (PSLR) is around 13.2 dB. From Fig. 4(d), we can see that the FWHM of the compressed signal is 594 ps and the PSLR is 13.2 dB. As far as an ideal LFMW with the same parameter as the generated X-band signal, the FWHM of the compressed pulse is about 295 ps and the PSLR is 13.2 dB. While from Fig. 5(d), we can see that the FWHM of the compressed signal is 296 ps and the PSLR is 13.2 dB. The FWHM and PSLR of the generated signals are close to that of the ideal signals, showing the generated signals have a good performance, which lays the foundation for the accuracy of coherent data fusion.

In the receiver, the OSRM described in the schematic diagram is realized by a PM-DMZM and a polarization beam splitter (PBS). The echo received by the HA is filtered by a multiple-channel filter. The signals from the S-band channel and X-band channel are separately amplified by a low-noise amplifier and then applied to a PM-DMZM (Fujitsu FTM7980EDA). Figure 3(b) shows the detailed structure of the PM-DMZM, which consists of two sub-MZMs, a PBS and a polarization beam combiner (PBC). The input optical signal from a PD is split into two orthogonal components in the PM-DMZM. Each component is used to complete the de-chirping processing for each band echo. The phase difference introduced by the bias voltage of each sub-MZM is set to be 0 or π. The output optical wave from the PM-DMZM is split by a PBS and sent to two PDs to perform the optical-to-electrical conversion. The de-chirped signals of S-band and X-band can be obtained after the high-frequency interference signal and the direct current signal are filtered by a BPF. Because the dual-band de-chirping processing is finished in a single PM-DMZM simultaneously and both

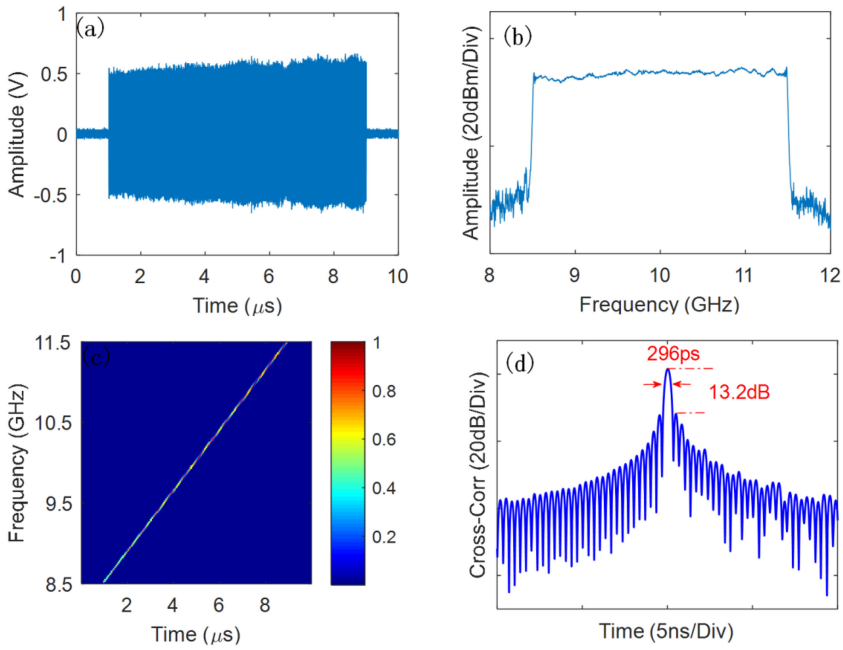

Fig. 5. Generation of the X-band LFMW with a bandwidth of 3 GHz (8.5–11.5 GHz), a pulse width of 8 μs and a period of 10 μs. (a) The waveform, (b) the spectrum, (c) the instantaneous frequency of the generated LFMW and (d) the cross-correlation peak.

the reference signals of each band are coherent, the dechirped signals still maintain a phase coherence. Then the signals are digitized by an oscilloscope (Agilent DSO81204B) simultaneously.

An experiment is performed to evaluate the ranging performance of the proposed dual-band radar system. Two metallic plane targets are placed on a wooden board, as shown in Fig. 6. Firstly, we adjust the farther metallic plane target and make it 20 cm far away from the closer one. The de-chirped signals of S-band and X-band are sampled and recorded utilizing the real-time oscilloscope working at a sampling rate of 100 MSa/s simultaneously. The fusion data can be obtained by performing coherent fusion processing without complex phase compensation due to the phase coherence of the de-chirped signals. The coherent fusion processing is mainly based on the algorithm presented in [25]. The range profiles of the targets obtained by S-band, X-band and fusion data are shown in Fig. 7(a). We can see that the two metallic plane targets are separated away obviously and the separation distances between them measured by the S-band, X-band and fusion data are 19.1 cm, 19.8 cm, and 19.9 cm separately, which matches well with the actual relative position. Then we move the farther metallic plane target closer to the other one. When they are separated by 10 cm, the two metallic plane targets can still be distinguished and the separation distances between them measured by S-band, X- band and fusion data are 10.6 cm, 8.6 cm, and 9.6 cm separately, as shown in Fig. 7(b). Furthermore, when they are separated by 5 cm, there is only one peak in the range profile obtained by S-band data, while there are two peaks in the range profiles obtained by X-band and fusion data and the separation distances between them are 5.2 cm, 4.9 cm separately, as shown in Fig. 7(c). In order to explore the ranging limitation of the fusion data, the distance between the two metallic plane targets is narrowed continually. When they are separated by 1.6 cm, they can not be distinguished either by S-band or by X-band data. While they can be distinguished by fusion data and the measured seperaion distance is 1.8 cm, as shown in Fig. 7(d).

From the ranging experiment, the S-band and X-band radar can distinguish two targets separated by 10 cm and 5 cm separately. While by coherent fusion processing of the dual-band signal, a super-resolution range profile of 1.6 cm can be realized, which is nearly equivalent to the resolution gotten by an LFMW signal with a bandwidth of 9.5 GHz ranging from 2 to 11.5 GHz.

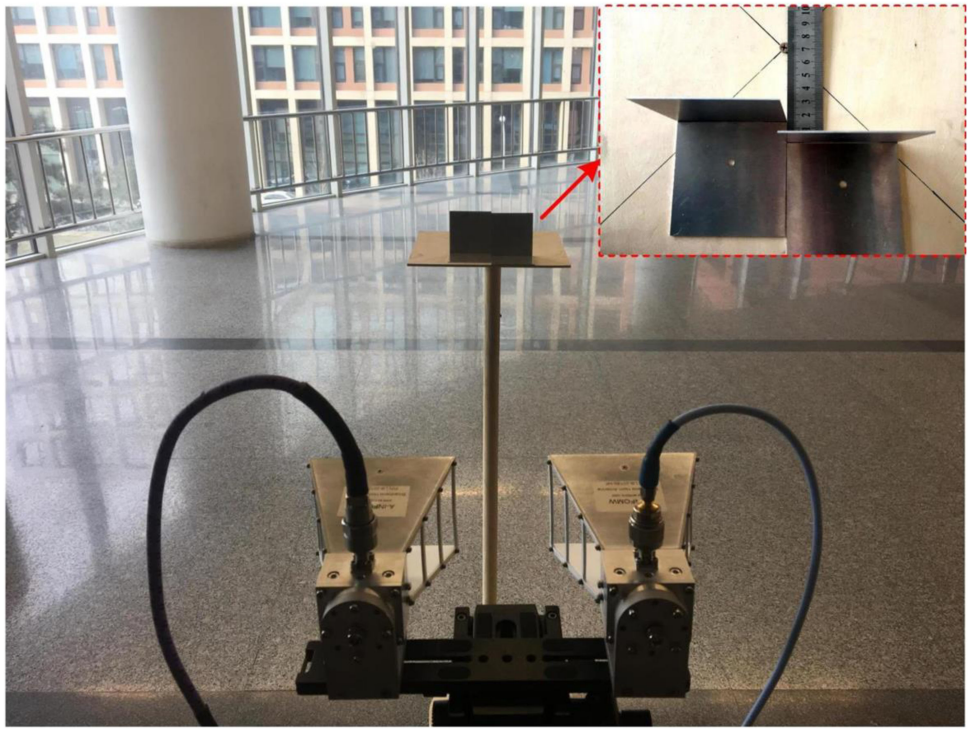

Fig. 6. Configuration for detecting two metallic plane targets.

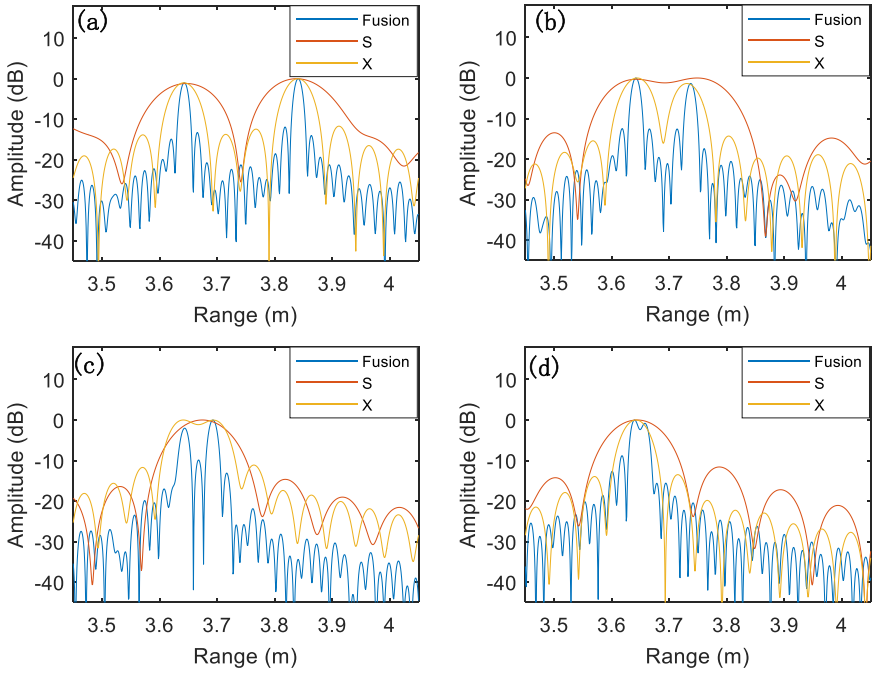

Fig. 7. The range information of the targets obtained by S-band (light red line), X-band (saffron yellow line) and fusion data (baby blue line) (a) the targets separated by 20 cm; (b) the targets separated by 10 cm; (c) the targets separated by 5 cm; (d) the targets separated by 1.6 cm.

4. Conclusion

We have presented and experimentally demonstrated a photonics-based dual-band radar for super-resolution range profile. This radar can generate and process coherent dual-band signals with large bandwidths simultaneously based on a compact single photonics-assisted transceiver. By coherent fusion processing of the sub-band signals, a super-resolution range profile can be obtained. In the experiments, a dual-band radar operating in S and X band is achieved. The S-band signal with a bandwidth of 1.5 GHz (2–3.5 GHz) and the X-band signal with a bandwidth of 3 GHz (8.5–11.5 GHz) are generated simultaneously. The dual-band echo is de-chirped through optical polarization multiplexing using a PM-DMZM, and a fusion data can be obtained by coherent fusion processing. A super-resolution of 1.6 cm is demonstrated in the scenario of two metallic plane targets by coherent fusion processing of the S-band and X-band signal. This technology shows a potential application in target recognition and identification.

References

[1] M. I. Skolnik, *Introduction to Radar*. New York, NY, USA: McGraw-Hill, 1962.
[2] V. C. Chen and M. Martorella, *Inverse Synthetic Aperture Radar Imaging: Principles, Algorithms, and Applications*. Herts, U.K.: SciTech, 2014.
[3] Q. Li, D. Yang, X. H. Mu, and Q. L. Huo, "Design of the L-band wideband LFM signal generator based on DDS and frequency multiplication," in *Proc. Int. Conf. Microw. Millimeter Wave Technol.*, 2004, vol. 4, pp. 1–4.
[4] A. Kaul, "Software defined radio: The transition from defense to commercial markets," in *Proc. Softw. Defined Radio Tech. Conf. Product Expo.*, 2007, pp. 1–7.
[5] P. Ghelfi *et al.*, "Photonics in radar systems: RF integration for state-of-the-art functionality," *IEEE Microw. Mag.*, vol. 16, no. 8, pp. 74–83, Sep. 2015.
[6] J. Capmany and D. Novak, "Microwave photonics combines two worlds," *Nature Photon.*, vol. 1, no. 6, pp. 319–330, 2007.
[7] J. Yao, "Microwave photonics," *J. Lightw. Technol.*, vol. 27, no. 3, pp. 314–335, Feb. 2009.
[8] F. Zhang *et al.*, "Photonics-based broadband radar for high-resolution and real-time inverse synthetic aperture imaging," *Opt. Exp.*, vol. 25, no. 14, pp. 16274–16281, 2017.
[9] R. Li, W. Li, M. Ding, Z. Wen, Y. Li, and L. Zhou, "Demonstration of a microwave photonic synthetic aperture radar based on photonics-assisted signal generation and stretch processing," *Opt. Exp.*, vol. 25, no. 13, pp. 14334–14340, 2017.
[10] J. Liao *et al.*, "Novel photonic radio-frequency arbitrary waveform generation based on photonic digital-to-analog conversion with pulse carving," in *Proc. Conf. Lasers Electro-Opt.*, 2015, pp. 1–2.
[11] S. Peng *et al.*, "High-resolution W-band ISAR imaging system utilizing a logic-operation-based photonic digital-to-analog converter," *Opt. Exp.*, vol. 26, no. 2, pp. 1978–1987, 2018.
[12] P. Ghelfi *et al.*, "A fully photonics-based coherent radar system," *Nature*, vol. 507, no. 7492, pp. 341–345, 2014.
[13] B. Gao, F. Zhang, Y. Yao, and S. Pan, "Photonics-based multiband radar applying an optical frequency sweeping comb and photonic dechirp receiving," in *Proc. Asia Commun. Photon. Conf.*, 2018, pp. 1–3.
[14] F. Scotti, F. Laghezza, P. Ghelfi, A. Bogoni, S. Pinna, and V. Vercesi, "Photonics-assisted dual band coherent radar system," in *Proc. Eur. Radar Conf.*, 2014, pp. 145–148.
[15] F. Scotti, F. Laghezza, P. Ghelfi, and A. Bogoni, "Multi-band software-defined coherent radar based on a single photonic transceiver," *IEEE Trans. Microw. Theory Techn.*, vol. 63, no. 2, pp. 546–552, Feb. 2015.
[16] P. Ghelfi, F. Laghezza, F. Scotti, D. Onori, and A. Bogoni, "Photonics for radars operating on multiple coherent bands," *J. Lightw. Technol.*, vol. 34, no. 2, pp. 500–507, Jan. 2016.
[17] F. Laghezza, F. Scotti, D. Onori, and A. Bogoni, "ISAR imaging of non-cooperative targets via dual band photonics-based radar system," in *Proc. Radar Symp.*, 2016, pp. 1–4.
[18] J. Yang, S. Li, X. Xiao, D. Wu, X. Xue, and X. Zheng, "Broadband photonic ADC for microwave photonics-based radar receiver," *Chin. Opt. Lett.*, vol. 16, no. 6, pp. 2018, Art. no. 060605.
[19] K. M. Cuomo, "A bandwidth extrapolation technique for improved range resolution of coherent radar data," Lincoln Lab., Massachusetts Inst. Technol., Cambridge, MA, USA, Project Rep. CJP-60, 1992.
[20] K. M. Cuomo, J. E. Piou, and J. T. Mayhan, "Ultra-wideband coherent processing," *Lincoln Lab. J.*, vol. 10, no. 2, pp. 203–222, 1997.
[21] C. Wang, W. Hu, X. Du, and W. Yu, "A new method of HRR profile formation based on multiple radars LFM signal fusion," in *Proc. 5th IEEE Int. Symp.*, 2005, pp. 131–135.
[22] C. Wang, W. Hu, X. Du, and W. Yu, "High resolution range profile formation based on LFM signal fusion of multiple radars," *Chin. J. Electron.*, vol. 24, no. 1, pp. 75–82, 2007.
[23] J. Tian, J. Sun, G. Wang, Y. Wang, and W. Tan, "Multiband radar signal coherent fusion processing with IAA and apFFT," *IEEE Signal Process Lett.*, vol. 20, no. 5, pp. 463–466, May 2013.
[24] H. Zhang and R. Chen, "Coherent processing and superresolution technique of multi-band radar data based on fast sparse Bayesian learning algorithm," *IEEE Trans. Antennas Propag.*, vol. 62, no. 12, pp. 6217–6227, Dec. 2014.
[25] B. Hussain *et al.*, "Performance analysis of auto-regressive UWB synthesis algorithm for coherent sparse multi-band radars," in *Proc. Int. Conf. Radar Syst.*, 2017, pp. 1–6.